




Article

In-Situ Characterization of Microstructural Changes in Alloy 718 during High-Temperature Low-Cycle Fatigue

Sebastian Barton ^{*}, Maximilian K.-B. Weiss  and Hans Jürgen Maier 

Institut für Werkstoffkunde (Materials Science), Leibniz Universität Hannover, An der Universität 2, 30823 Garbsen, Germany

* Correspondence: barton@iw.uni-hannover.de

Abstract: Components made of nickel-based alloys are typically used for high-temperature applications because of their high corrosion resistance and very good creep and fatigue strength, even at temperatures around 1000 °C. Corrosive damage can significantly reduce the mechanical properties and the expected remaining service life of components. In the present study, a new method was introduced to continuously determine the change in microstructure occurring as a result of exposure to high temperature and cyclic mechanical loading. For this purpose, the conventional low-cycle fatigue test procedure was modified and a non-destructive, electromagnetic testing technique was integrated into a servohydraulic test rig to monitor the microstructural changes. The measured values correlate with the magnetic material properties of the specimen, allowing the microstructural changes in the specimen's subsurface zone to be analyzed upon high-temperature fatigue. Specifically, it was possible to show how different loading parameters affect the maximum chromium depletion as well as the depth of chromium depletion, which influences the magnetic properties of the nickel-based material. It was also observed that specimen failure is preceded by a certain degree of microstructural change in the subsurface zone. Thus, the integration of the testing technology into a test rig opens up new possibilities for improved prediction of fatigue failure via the continuous recording of the microstructural changes.



Citation: Barton, S.; Weiss, M.K.-B.; Maier, H.J. In-Situ Characterization of Microstructural Changes in Alloy 718 during High-Temperature Low-Cycle Fatigue. *Metals* **2022**, *12*, 1871. <https://doi.org/10.3390/met12111871>

Academic Editors: Martin Heilmaier and Martina Zimmermann

Received: 7 October 2022

Accepted: 25 October 2022

Published: 2 November 2022

Publisher's Note: MDPI stays neutral with regard to jurisdictional claims in published maps and institutional affiliations.



Copyright: © 2022 by the authors. Licensee MDPI, Basel, Switzerland. This article is an open access article distributed under the terms and conditions of the Creative Commons Attribution (CC BY) license (<https://creativecommons.org/licenses/by/4.0/>).

Keywords: alloy 718; fatigue; oxidation; chromium depletion; non-destructive testing

1. Introduction

Components in aircraft, aerospace, industrial, and automotive engineering are frequently subjected to severe loads due to thermal fluctuations and cyclic mechanical stresses. In order to ensure a sufficient service life under these loading conditions, these components are often manufactured using nickel-based alloys, the so-called superalloys. These alloys exhibit very high resistance to corrosion, as well as high creep and fatigue strength, even at temperatures around 1000 °C. Their excellent properties at these high temperatures are achieved by alloying up to 15 elements with nickel as the base element. High mechanical strength is reached in particular by the formation of ordered precipitates and carbides. Corrosion protection is provided by alloying with sufficiently high contents of the coating-forming elements chromium and aluminum [1–4].

A component's service life is often determined by mechanical and corrosive factors. The high temperatures and an oxygen-containing atmosphere lead to oxidation of the component surface. If the chromium and aluminum contents are sufficiently high, protective coating layers are formed that drastically slow down further oxidation and typically, parabolic oxide layer growth occurs. As the protective layer forming elements diffuse from the component subsurface to the component surface, the component subsurface becomes depleted in these elements. If the subsurface is excessively depleted in these elements, the oxide layer can no longer be re-established in the event of local damage. As a result, the protective effect of the oxide layer is finally lost. Cyclic mechanical stress acting on the

component can lead to such local damage in form of cracks in the protective oxide layers. Due to the constant reformation of the oxide layer, the element depletion in the component subsurface increases rapidly. If the oxide layers no longer provide sufficient protection, oxidation products may form in the material and on grain boundaries. This can lead to notch effects, crack initiation, and component failure [5–8].

The depletion of alloying elements can also lead to a change in the magnetic material properties. In fact, an initially paramagnetic material behavior can change to a ferromagnetic one. This effect makes it possible to detect microstructural changes as a result of high-temperature corrosion using non-destructive testing (NDT) techniques [9–14]. Harmonic analysis of eddy current signals (EC-HA) is a non-destructive testing technique suitable for characterizing such changes in the magnetic material properties. This testing technique is mostly used for non-destructive characterization of steel alloys with ferromagnetic properties [15–17]. For detecting microstructural changes in nickel-based superalloys by EC-HA, the fact can be exploited that the chromium depletion correlates with the Curie temperature and the amplitude of the third harmonic at 25 °C [18–20]. In the context of the present study, EC-HA was integrated into a servohydraulic test rig in order to record the change of the specimen subsurface zone under high-temperature fatigue conditions in a non-destructive manner.

There are various test techniques for assessing the behavior of high-temperature materials under thermal and mechanical loading conditions. These can be divided into isothermal, thermo-mechanical, or thermal fatigue tests [21–24]. The objective of the present study was to evaluate an EC-HA system designed to monitor the microstructural degradation in the subsurface region under such conditions. Although the present study was limited to isothermal high-temperature low-cycle fatigue (LCF) test, the approach is applicable to other loading scenarios as well.

2. Materials and Methods

The experiments were carried out using the nickel-based alloy 718 in annealed condition. The alloy composition was 18.6 wt.% Fe, 18.4 wt.% Cr, 5.1 wt.% Nb, 2.9 wt.% Mo, 0.9 wt.% Ti, 0.5 wt.% Al, 0.3 wt.% Co, and balance Ni. For testing, cylindrical specimens with a diameter in the gauge section of 8 mm were employed. The samples were tested in the as-machined condition (surface roughness of $R_z = 2 \mu\text{m}$).

The modified isothermal LCF tests were performed on an MTS Landmark 370.10 servohydraulic universal test system (MTS Systems Corp., Eden Prairie, MN, USA). The key components of the test set-up are presented in Figure 1. The LCF parts of the tests were conducted in total strain control with triangular wave shape and a test frequency of 0.0083 Hz. The actual strain was measured by a high-temperature extensometer (MTS Systems Corp., Eden Prairie, MN, USA) attached to the specimen. The specimen was heated inductively via an induction coil enclosing the specimen. The temperature of the specimen was determined without contact via a pyrometer. To ensure a constant emission coefficient of the specimen surface, the specimen was painted black with heat-resistant paint. The temperature measurements were calibrated using thermocouples attached to companion specimens.

The EC-HA system was integrated into the fatigue test rig, allowing in-situ electromagnetic characteristics to be monitored as shown in Figure 1. Specifically, a temperature-resistant EC-HA tactile sensor (in-house development) was used to record the magnetic properties. Protection against high specimen temperatures was realized by a thin-walled housing made of a paramagnetic, low-conductive metal. The sensor was operated at a frequency of 1.6 kHz and had a measuring spot diameter of 15 mm. Therefore, not the entire sample was probed, but only a selected part of the sample. The penetration depth and the volume probed are essentially dependent on the electrical and magnetic material properties in addition to the selected test frequency. Since alloy 718 has paramagnetic properties in its initial state as well as a low electrical conductivity (approx. 1 MS/m), high penetration depths result. In fact, for the geometry used it would also be possible to

detect the formation of ferromagnetic phases on the backside of the sample. However, this changes when a thin, ferromagnetic surface layer forms as a result of high-temperature oxidation. Then the effective penetration depth decreases to a few μm . To position the sensor on the specimen, a linear axis with a spindle drive and a traverse path of 250 mm was used. With the traversing unit, the sensor was moved from a position outside the effective field of the inductor (= parking position) to the specimen (= measuring position). By means of an integrated spring mechanism, the sensor was pressed onto the specimen surface with a constant force when the sensor was in the measuring position.

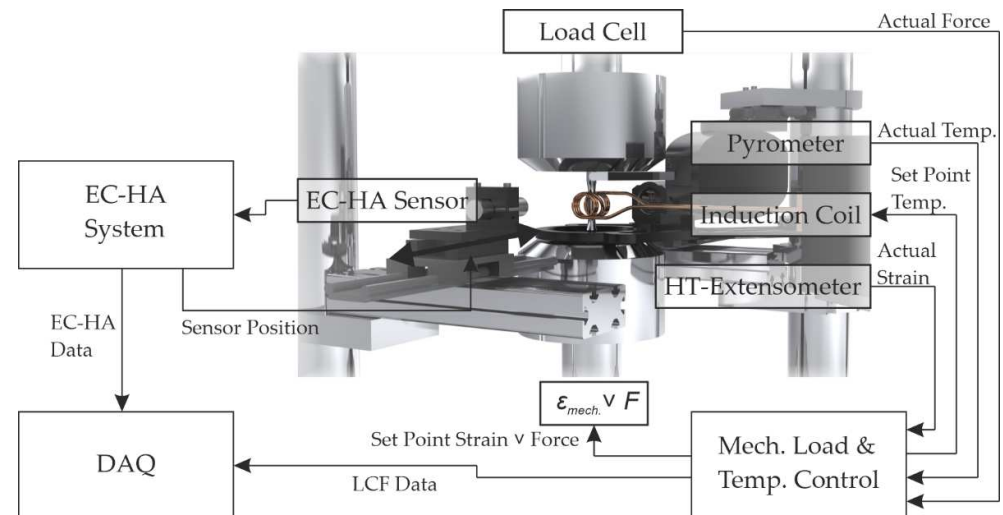


Figure 1. Schematic illustration of the LCF test rig and the integrated non-destructive EC-HA testing system.

As described in ref. [18], the Curie temperature and the amplitude of the third harmonic can be used to evaluate the microstructural state of the subsurface zone. In order to reduce the number of influencing factors in the test sequence, only isothermal, strain-controlled LCF tests were carried out in the present study. The actual test sequence is shown in Figure 2. It consists of a conventional high-temperature LCF part and a cooling/measuring period. At the beginning of each test cycle, the specimen was heated to the target temperature of 800 °C in the gauge section while the stress in the specimen was controlled at 0 MPa, allowing the specimen to expand freely during heating. At the end of heating, a holding phase of 120 s was used to minimize temperature gradients in the gauge length. Thereafter, the specimen strain was set to 0%. Then strain-controlled mechanical loading commenced, using a triangular wave shape. After a defined number of load cycles, heating was turned off and the samples was cooled down in stress control to allow specimen stress-free thermal contraction. When the specimen temperature dropped below 450 °C, the EC-HA sensor was moved from the parking position to the measuring position, Figure 2b. The EC-HA signal was then recorded until the sample temperature dropped below 25 °C. The duration of the cooling of the samples to a value < 25 °C was about 10 min. Thereafter, the EC-HA sensor was retracted and heating to the next LCF cycle began.

The entire test was terminated when the peak stress at maximum strain dropped to a level below 50% of the one in the saturation regime. At such a large stress drop clearly detectable crack growth had occurred. The experimental parameters used in the fatigue tests are summarized in Table 1. The temperature specified in Table 1 is the set temperature. In all three tests, an average temperature of 798 °C was measured during the high-temperature LCF part, with temperature variations within the gage length remaining within the permissible limits according to ASTM E 606.

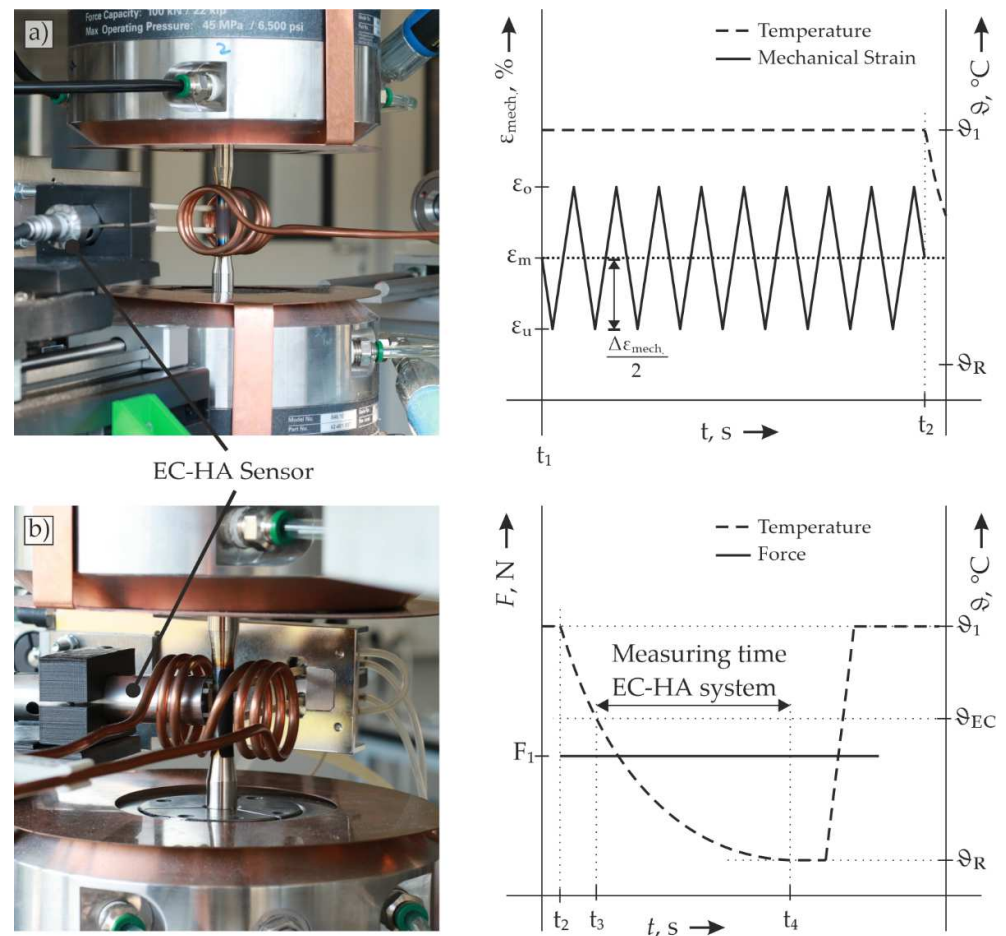


Figure 2. Modified LCF test procedure with combined EC-HA measurement: (a) strain-controlled LCF at a constant temperature of ϑ_1 with EC-HA sensor in park position, (b) EC-HA sensor in measurement position recording the electromagnetic characteristics of the specimen between ϑ_{EC} and ϑ_R under stress-free conditions ($F_1 = 0$).

Table 1. Test parameters of the modified isothermal LCF tests.

Specimen	Temperature ϑ_1 , °C	Total Strain Amplitude $\Delta\epsilon_{\text{mech},2}$, %	Duration per Load Cycle, s	Load Cycles per Test Cycle, -
1	800	0.3	120	20
2	800	0.5	120	20
3	800	0.7	120	20

The magnet-inductive testing method of harmonic analysis of eddy current signals was designed such as to be most sensitive for the detection of ferromagnetic phases and for the evaluation of the changes caused by high-temperature oxidation. Specifically, the microstructural changes in the specimen subsurface zone were determined by evaluating the amplitude of the third harmonic as a function of the specimen temperature. The details of the NDT technique are given in Ref. [18].

Ferromagnetic phases show a ferromagnetic behavior until the so-called Curie Temperature reached. Once this temperature is exceeded, a former ferromagnetic phase becomes paramagnetic. According to the procedure described in ref. [18], the Curie temperature of the sample can be determined by defining a threshold value in the amplitude of the third harmonic. This threshold value can be correlated with the maximum chromium depletion in the subsurface zone, see Figure 3a, since a reduction in chromium content

leads to a ferromagnetic behavior of the nickel-based alloy 718. Thus, the value of the amplitude of the third harmonic at a temperature of 25 °C can be correlated with the depth of chromium depletion, cf. Figure 3b. By monitoring the amplitude of the third harmonic over the specimen temperature after each test cycle, the change in microstructure in the specimen subsurface zone up to specimen failure can be non-destructively detected. Since in the described experimental setup the minimum sample temperature corresponds to the room temperature (≈ 25 °C), no Curie temperatures below 25 °C were detected in the experiments conducted in the present study.

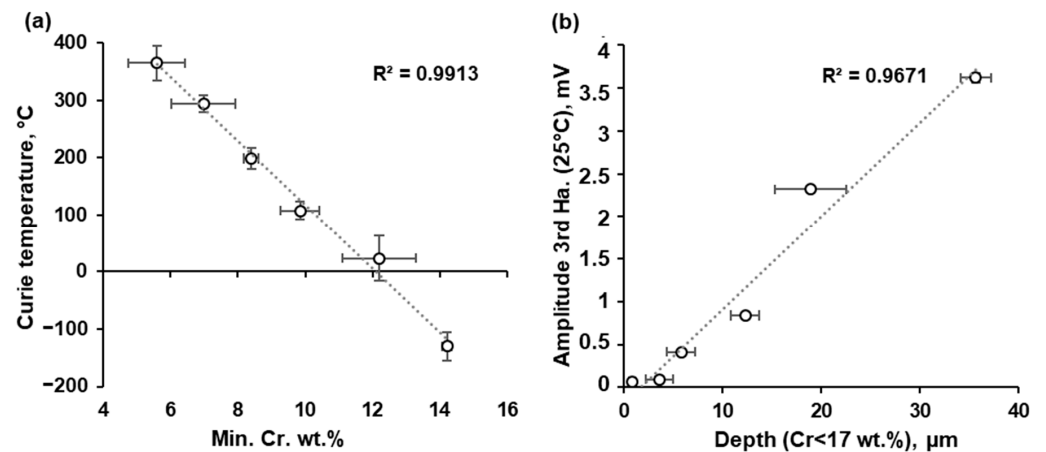


Figure 3. (a) Minimum Cr content vs. Curie temperature and (b) size of the chromium-depleted subsurface region vs amplitude of the third harmonic Reprinted with permission from ref. [18]. Copyright 2022 Taylor & Francis.

In conjunction with the recording of the electromagnetic measurements, the specimens were examined with regard to the microstructural changes occurring in the subsurface region. For this purpose, the specimens were cut along the longitudinal axis, with the cut being aligned such that its plane passed through the measuring spot of the EC-HA sensor. The specimens were then embedded in electrically conductive resin and polished. Element mappings by energy dispersive spectroscopy using X-rays (EDX) were obtained using a XV-scanning electron microscope (SEM) Mira VP (VisiTec Mikrotechnik GmbH, Grevesmühlen, Germany) operated at an acceleration voltage of 20 kV to determine the element distribution around the crack initiation site.

3. Results

In Figure 4 the change of the Curie temperature, observed via the change in the amplitude of the third harmonic as a function of the specimen temperature for different loading cycles is displayed. After the first test cycle, i.e., 20 individual load cycles, the amplitude signal cannot be distinguished from the baseline noise, which shows that the Curie temperature is lower than 25 °C. At 374 cycles, which corresponded to 27% of the fatigue life, the pre-defined amplitude threshold value of 1.5 times the baseline noise for determining the current Curie temperature was exceeded. As seen in Figure 4, a clear increase in the amplitude of the third harmonic, i.e., an increase in the Curie temperature can be seen after 520 load cycles. The 520 load cycles correspond approximately to 37.5 % of fatigue life. As cycling progresses, both the amplitude of the third harmonic, and thus the Curie temperature continued to increase. After 1380 cycles, shortly before reaching the end of the fatigue test a 1382 cycles, the amplitude of the third harmonic showed a value of 0.43 mV and the Curie temperature amounted to 110 °C.

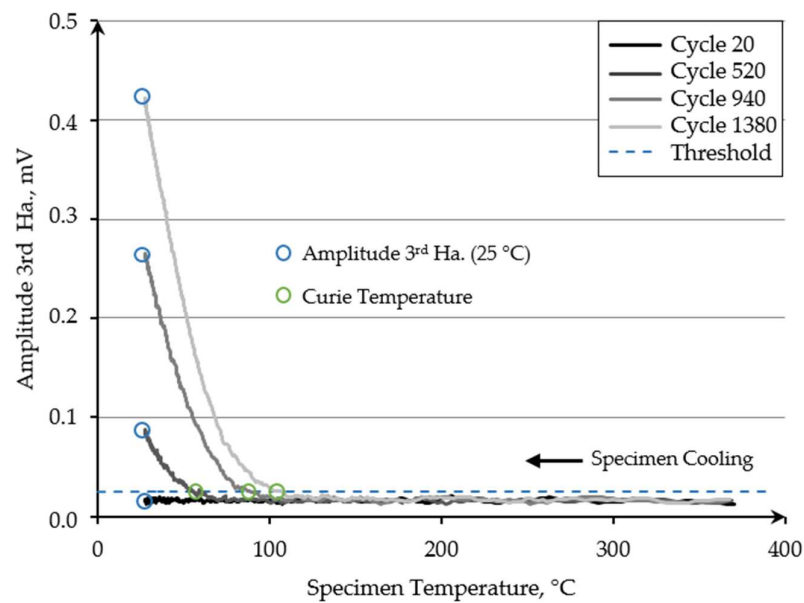


Figure 4. Amplitude of the third harmonic versus specimen temperature for selected cycles in the modified isothermal LCF test with a strain amplitude of $\epsilon_{\text{mech.}} = 0.5\%$, a strain ratio of $R_{\epsilon} = -1$ and a specimen test temperature of $\vartheta_1 = 800\text{ °C}$.

Figure 5 shows selected stress-strain hysteresis loops from the specimen used to monitor the changes in the third harmonic in Figure 4. Whereas the latter has already revealed a detectable microstructural change at 374 cycles (27% of fatigue life), the effect of crack growth on apparent stress–strain response is only apparent clearly close to the end of the test in Figure 5e), where the maximum stress was seen to decrease substantially, and the hysteresis loop began to show an inclination in the compressive part. Both effects demonstrated that substantial crack formed at this stage.

The potential to detect fatigue damage early on via EC-HA is further evaluated in Figure 6, which shows the course of the amplitude of the third harmonic and the Curie temperature as a function of fatigue life. Here, a clearly detectable increase of the amplitude of the third harmonic can be seen at about 25% fatigue progress, which corresponds to the microstructural change in the probed subsurface layer. The calculated change in Curie temperature corresponds to a substantial depletion in local chromium content.

By tracking the electromagnetic parameters during fatigue, insight can be gained into damage evolution. Figure 7 shows the progress of the Curie temperatures of the three samples considered during the fatigue tests. As expected, the specimen strained with the highest amplitude fails at the lowest number of cycles. The curves of the specimens with strain amplitudes of 0.3% and 0.7% revealed a sharp increase in the Curie temperature in the cycles shortly before failure occurred. A better comparison is obtained plotting the Curie temperatures vs. the normalized fatigue life, cf. Figure 7b. Between a Curie temperature of 85 °C and 105 °C all specimens reached about 80% of fatigue life, irrespective of their actual strain amplitude.

In addition to the Curie temperatures, the amplitudes of the third harmonic curves at 25 °C were evaluated. As the Curie temperature reflects a different part of the data provided by tracking the third harmonic, the curves shown in Figure 8 progress differently.

Similar to Figure 7, the curves in Figure 8a are steeper at higher strain amplitudes. However, normalization, cf. Figure 8b, does not collapse the data onto a common master curve. This difference can be explained based on the total duration of the fatigue test. At lower strain amplitude, the samples are exposed to the high-temperature phase for more cycles, allowing changes in the microstructure as a result of high-temperature oxidation to take place over a longer duration. Thus, the increase in the amplitude of the third harmonic, normalized to the fatigue life, is greatest with a strain of 0.3%, i.e., for the sample with

longest test period. A longer testing time leads to greater chromium depletion and thus more ferromagnetic material, which is reflected by the increase in the amplitude of the third harmonic.

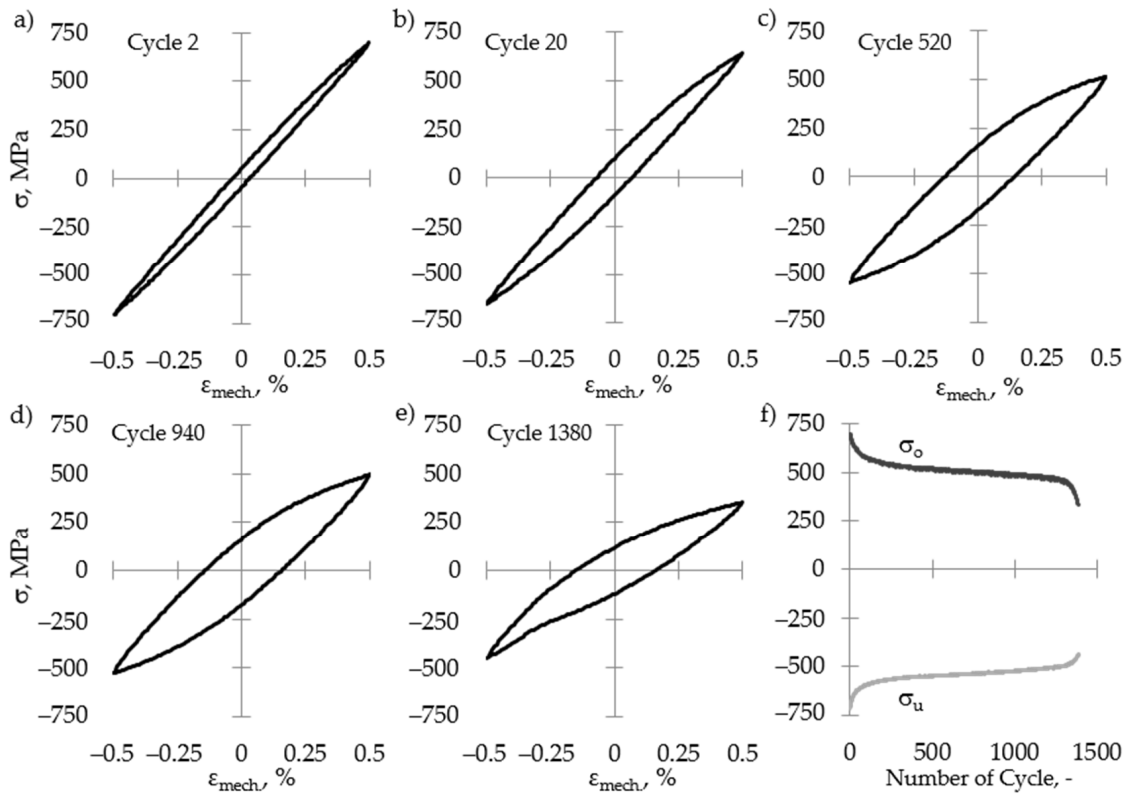


Figure 5. Stress–strain hysteresis loops after (a) 2 cycles, (b) 20 cycles, (c) 520 cycles, (d) 940 cycles, (e) 1380 cycles, and (f) maximum and minimum stress vs number of cycles for the fatigue test corresponding to Figure 4.

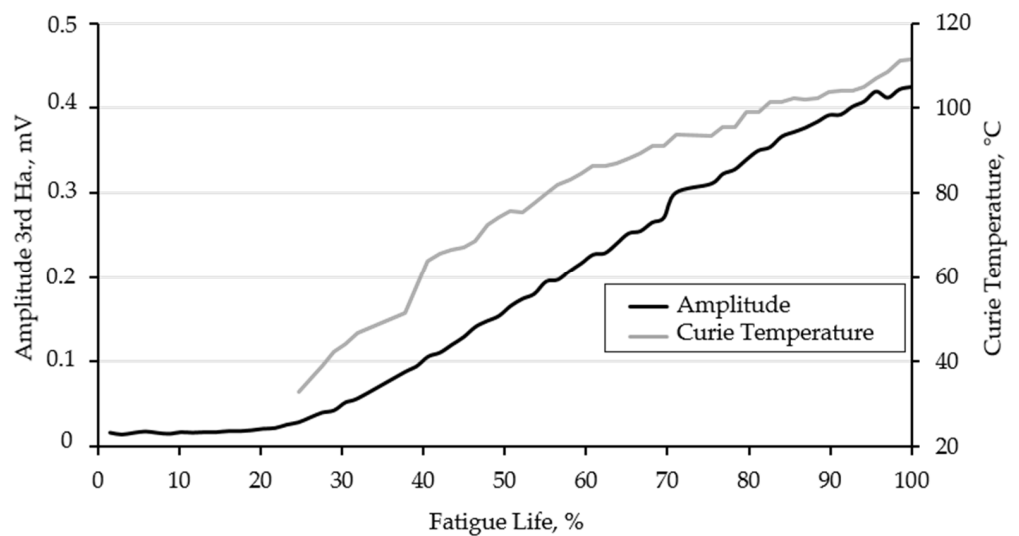


Figure 6. Amplitude of the third harmonic and Curie temperature versus fatigue life of the specimen subjected to 0.5% strain amplitude at 800 $^{\circ}C$.

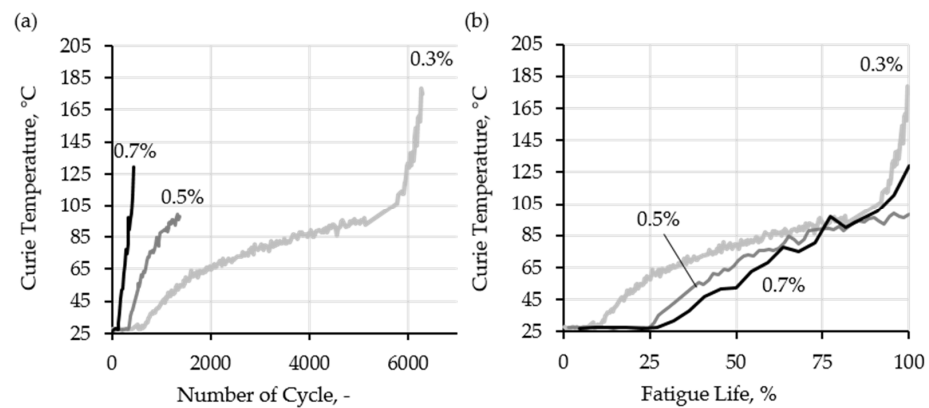


Figure 7. Evolution of Curie temperature in the fatigue tests with different strain amplitudes as a function of (a) the number of cycles and (b) normalized fatigue life; recompiled from ref. [19].

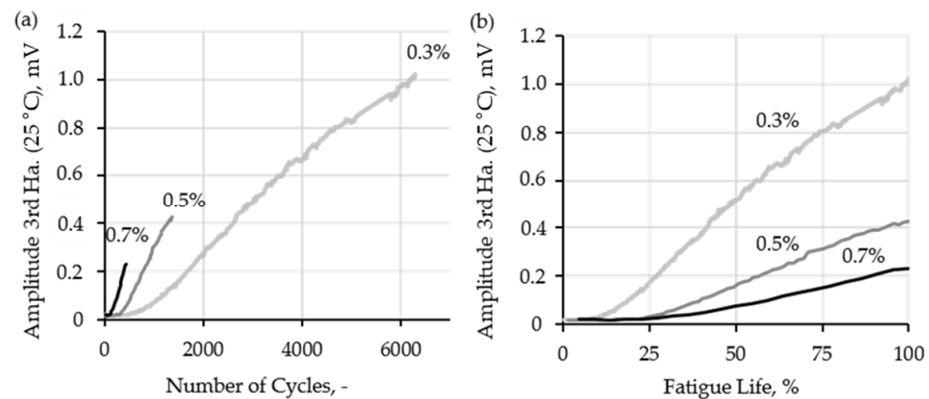


Figure 8. Evolution of the amplitude of the third harmonic at 25 °C in fatigue tests with different strain amplitudes as a function of (a) the number of cycles and (b) normalized fatigue life; recompiled from ref. [19].

To investigate the influence of high-temperature oxidation in more detail, micrographs were taken from the fatigued specimens around the cracked area. Optical microscope images showed that in addition to the primary crack which led to the specimen failure, further smaller cracks were induced, Figure 9. In the specimen with the longest test duration, Figure 9a, these secondary, smaller cracks were most pronounced.

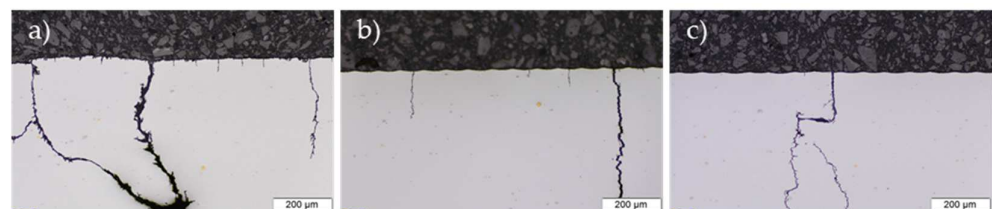


Figure 9. Optical microscope images of the fatigued specimens in the region of crack initiation: (a) 0.3%, (b) 0.5%, and (c) 0.7% strain amplitude.

EDX mappings for the element chromium showed the formation of a chromium-rich oxide layer, cf. Figure 10. Increased chromium content at the cracks surfaces, although less pronounced, was also seen. This is confirmed by the in the mapping of oxygen. High concentrations of oxygen were found at the surface and the crack flanks. This indicates the formation of oxides on the crack flanks. In addition, a chromium-depleted near surface zone was visible. This is most evident in the specimens that were subjected to 0.3% (1) and 0.7% (3) strain. In the specimen subjected to 0.5% strain (2), chromium depletion on the

crack flank was very weak. The mappings for the elements nickel and iron did not show any special peculiarities.

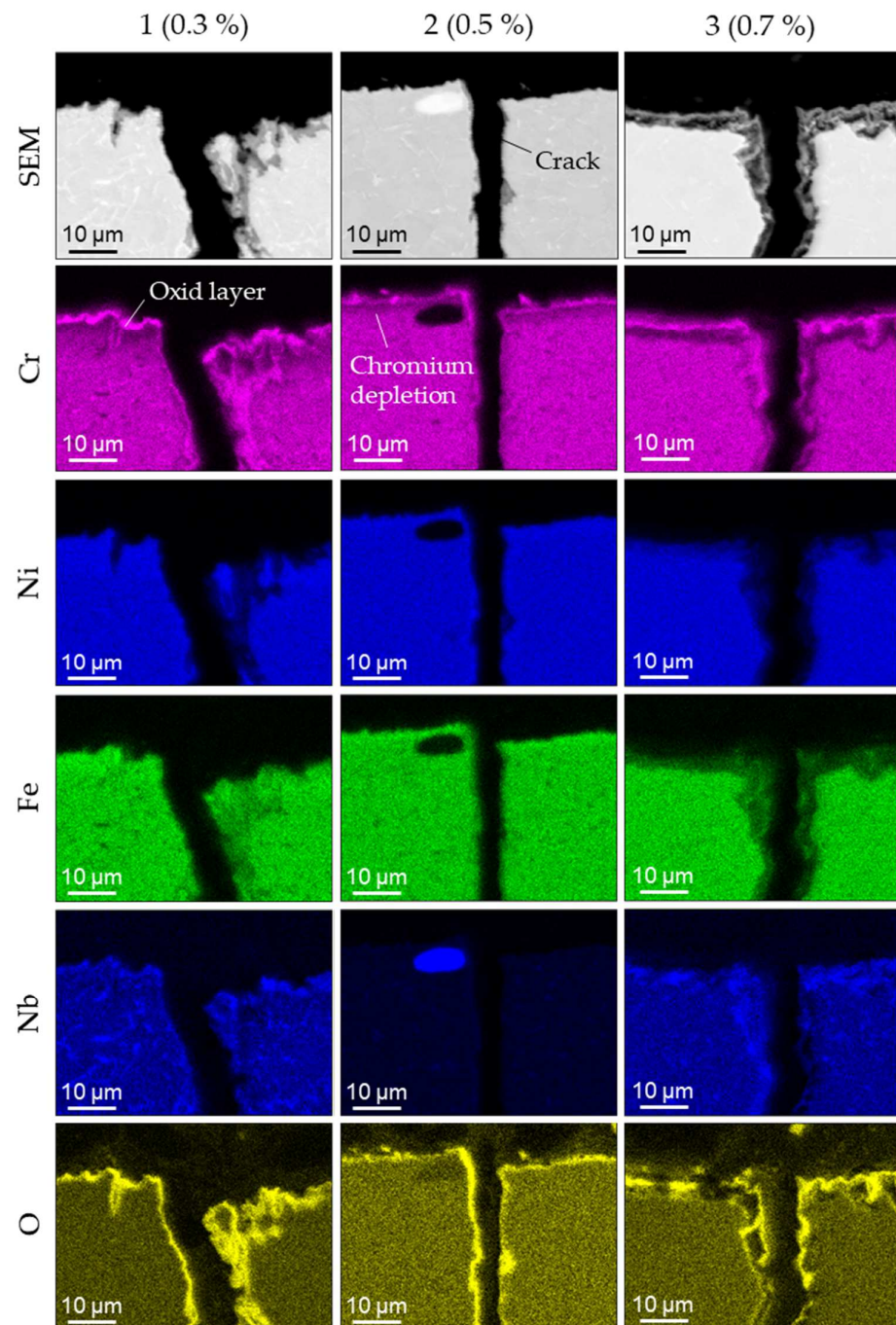


Figure 10. SEM images and EDX mappings for the elements chromium, nickel, iron, niobium, and oxygen.

Subsequently, as shown in Figure 11a, EDX line scans were taken from the specimen surface towards the center of the specimen and from the crack start diagonally into the interior of the specimen. Upon initial crack formation, the exposed substrate no longer features a protective coating. Subsequently, the oxides form, which increases the chromium depletion. This became more pronounced with increasing test duration as this process is controlled by diffusion. Thus, EDX analysis demonstrated that the depth affected by chromium depletion was larger in the case of the specimen cycled at a strain amplitude of 0.3%, cf. Figure 11c. By contrast, the chromium concentration profiles measured at the un-

cracked surface, Figure 11b, were much more similar. This difference can be explained if it is assumed that material transport is more rapid in the crack wake because of pipe-diffusion in the plastically deformed region.

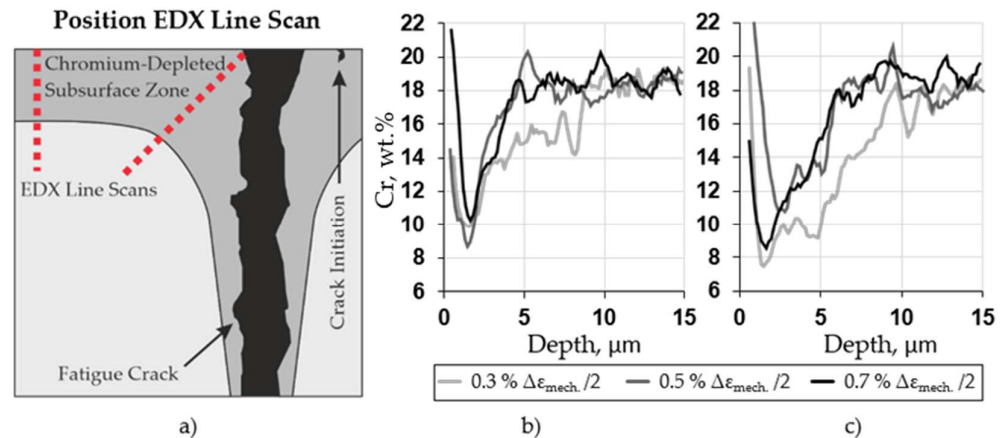


Figure 11. (a) Schematic illustration of the chromium-depleted zones and traces of the EDX line scans marked in red for scans from (b) the un-cracked surface to the center and (c) at the crack initiation site.

4. Discussion

The fatigue life of a cyclically loaded material can be divided into two parts: (i) the fraction of cycles required to initiate cracking and (ii) the fraction of cycles responsible for crack propagation [25]. In the crack initiation phase, a material can cyclically harden, soften, or exhibit an almost constant stress–strain response under cyclic loading. This depends, in part, on the material, the induced stress states, temperature, and type of fatigue test [26–28]. Corrosion-induced damage can have a substantial influence on crack initiation and early crack growth, which subsequently leads to fatigue failure. For example, many studies on crack growth during high-temperature fatigue of alloy 718 show that crack growth rates in tests conducted in air are significantly higher than those conducted in vacuum. Especially in tests with low test frequencies, as in the present study, high-temperature oxidation has a great influence on the crack growth rate [29–33].

The high-temperature oxidation of alloy 718 manifests itself, in particular, in a pronounced depletion of the subsurface zone in chromium. Chromium depletion as a result of high-temperature oxidation in alloy 718 has been studied using metallography by many authors, e.g., refs. [34–36]. In the present study, the amplitude of the third harmonic of EC-HA testing was used, which senses the volume of material affected by chromium depletion, and the Curie temperature determined, correlates with the maximum depth of chromium depletion. In this way, the progress of high-temperature corrosion can be evaluated non-destructively [18]. By implementing the EC-HA testing system into an isothermal LCF test rig, an estimate of the remaining fatigue life is possible, cf. Figure 7b. From a mechanistic point of view, this is based on the newly created surfaces upon crack initiation and early crack growth and hence accelerated chromium depletion.

It was shown that chromium depletion is not only dependent on time and temperature but also on cyclic straining. The electromagnetically measured data have shown that both the maximum chromium depletion and the depth of chromium depletion increase more rapidly with cycle number at larger strain amplitude, cf. Figures 7 and 8. The EDX line scans also show that the maximum chromium depletion occurs at the site of crack initiation, Figure 11. During crack growth, an unprotected surface forms in the already depleted subsurface zone. This leads to significantly accelerated chromium depletion. This is also evident in the Curie temperature curves. This explains the strong increase in the Curie temperature for sample 1 ($\Delta\epsilon_{\text{mech.}}/2 = 0.3\%$) that occurred at approx. 80% of the test duration, when more and/or larger cracks form, cf. Figure 7. For sample 3 ($\Delta\epsilon_{\text{mech.}}/2 = 0.7\%$), the same trend was seen close to the end of fatigue life, but the effect

is less pronounced. This is to be expected as at the higher mechanical strain amplitude crack growth is faster, and thus exposure time of the unprotected surfaces is shorter. Yet, sample 2 ($\Delta\varepsilon_{\text{mech.}}/2 = 0.5\%$) did not show such a sharp increase close to failure. In this sample, crack initiation did not take place in the area probed by the measuring spot of the sensor. The crack only grew into the measuring area just before final failure. Consequently, high-temperature oxidation could only act briefly on the open crack flank in the area probed by the sensor. Thus, there was only a small additional decrease of the minimum chromium content in this area and no further increase of the Curie temperature was seen in the data. In summary, the change in the signal depends both on the strain amplitude and the crack initiation site with respect to the location of the sensor.

The integration of electromagnetic testing technology into loading devices has already been reported, but the focus was on detecting martensitic transformations [37,38]. The application in high temperature LCF tests has not been described so far. The present results showed that by applying the NDT technique of harmonic analysis of eddy current signals at regular intervals, an estimation of the remaining service life can be made. Interestingly, normalization of the recorded electromagnetic data in terms of relative fatigue life, cf. Figure 7, shows that for the material studied at a Curie temperature of approx. $90\text{ }^{\circ}\text{C}$, about 20% residual service life remains independent of the mechanical loading. Such high Curie temperatures are straightforward to detect. Thus, by continuously monitoring the magnetic properties, it is possible to detect and evaluate a change in the material even at low damage states. This characteristic makes the non-destructive testing technique presented here potentially interesting as a test method for components in order to estimate their remaining service life.

As can be seen in Figure 9, the thermal and mechanical loadings induced a large number of cracks. Clearly, the first crack formed is not necessarily the one that leads to unstable crack growth, which then determines fatigue failure [30,39]. It is rather the case that several small incipient cracks occur, which then do not go beyond the stable crack growth regime. As with the primary crack, high-temperature corrosion acts on the open flanks that form in these cracks. This accelerates chromium depletion in these regions. These microstructural changes caused by high-temperature fatigue are also detected by EC-HA.

In order to determine and evaluate the microstructure of the subsurface layer by means of the presented method, the Curie temperature and the amplitude of the third harmonic must be determined repeatedly. For this purpose, phases in which the specimen cools down from the test temperature must be integrated into the test sequence. For actual components, shutdown periods may be exploited for such measurements. With respect to modeling fatigue life, it should be noted that cooling and reheating can cause stresses in the protective oxide layers, which can also lead to cracks. This can accelerate the environmental attack. Thus, the exact influence of the modified test procedure on the results of the fatigue tests have to be investigated in further studies. It should also be possible to transfer the findings to tests on thermomechanical or thermal fatigue tests. Provided that phases in which the specimen cools down to temperatures $< 100\text{ }^{\circ}\text{C}$ can be integrated, the current test procedure is straightforward to apply.

The investigations presented were carried out on samples of alloy 718. Transferability to other nickel- or cobalt-based alloys is likely. Specifically, these alloys must feature substantial changes in magnetic material properties as a result of high-temperature corrosion. This is particularly the case for alloys with high chromium contents. Chromium strongly reduces the Curie temperature in nickel-based alloys [40] and cobalt-based alloys [41]. Thus, a significant change in the local alloy composition can be expected in these alloys as a result of high-temperature corrosion, which in turn results in a change in the magnetic properties.

5. Conclusions

By using an electromagnetic non-destructive testing (NDT) technique, integrated into a modified, isothermal low-cycle fatigue (LCF) test rig, it was possible to estimate the residual specimen lifetime by measuring the change of the magnetic sample properties.

The change of the magnetic properties is caused by a chromium depletion, which changes the magnetic properties of the nickel alloy from paramagnetic to ferromagnetic. Dependent on the chromium content, the Curie temperature individually changes. In the present study, the change in the Curie temperature was detected by the NDT technique in-situ. Once a crack is formed, the newly created surface accelerates the chromium depletion and hence increases the Curie temperature. If the remaining chromium content is too low, no further corrosion protection is given and hence the service lifetime is reduced significantly in a high-temperature corrosive environment. This can be detected earlier in the electromagnetic testing signals as compared with monitoring the stress–strain response in the LCF test. Thus, the NDT data can be used for modeling residual service life as well as for gaining deeper insights into the crack propagation at high-temperature fatigue in high-temperature corrosion environments.

Author Contributions: Conceptualization, S.B., M.K.-B.W. and H.J.M.; methodology, S.B., M.K.-B.W. and H.J.M.; validation, S.B., M.K.-B.W. and H.J.M.; formal analysis, S.B., M.K.-B.W. and H.J.M.; investigation, S.B., M.K.-B.W. and H.J.M.; writing—original draft preparation, S.B. and M.K.-B.W.; writing—review and editing, S.B. and H.J.M.; visualization, S.B., M.K.-B.W. and H.J.M.; supervision, S.B. and H.J.M.; project administration, S.B.; funding acquisition, H.J.M. All authors have read and agreed to the published version of the manuscript.

Funding: This research was funded by the Deutsche Forschungsgemeinschaft (DFG, German Research Foundation) –SFB 871/3 –119193472.

Institutional Review Board Statement: Not applicable.

Informed Consent Statement: Not applicable.

Data Availability Statement: Data are available upon request.

Acknowledgments: The authors thank Deutsche Forschungsgemeinschaft for financial support. The publication of this article was funded by the Open Access Fund of the Leibniz Universität Hannover.

Conflicts of Interest: The authors declare no conflict of interest.

References

1. Xia, W.; Zhao, X.; Yue, L.; Zhang, Z. A review of composition evolution in Ni-based single crystal superalloys. *J. Mater. Sci. Technol.* **2020**, *44*, 76–95. [[CrossRef](#)]
2. Campbell, F.C. Superalloys. In *Manufacturing Technology for Aerospace Structural Materials*; Elsevier: Amsterdam, The Netherlands, 2006; pp. 211–272, ISBN 9781856174954.
3. Reed, R.C. *The Superalloys*; Cambridge University Press: Cambridge, UK, 2009; ISBN 9780521859042.
4. Pettit, F.S.; Meier, G.H. Oxidation and Hot Corrosion of Superalloys. In Proceedings of the Superalloys 1984 (Fifth International Symposium), Superalloys, Champion, PA, USA, 7–11 October 1984; pp. 651–687.
5. Li, X.; Li, W.; Imran Lashari, M.; Sakai, T.; Wang, P.; Cai, L.; Ding, X.; Hamid, U. Fatigue failure behavior and strength prediction of nickel-based superalloy for turbine blade at elevated temperature. *Eng. Fail. Anal.* **2022**, *136*, 106191. [[CrossRef](#)]
6. Stinville, J.C.; Martin, E.; Karadge, M.; Ismonov, S.; Soare, M.; Hanlon, T.; Sundaram, S.; Echlin, M.P.; Callahan, P.G.; Lenthe, W.C.; et al. Fatigue deformation in a polycrystalline nickel base superalloy at intermediate and high temperature: Competing failure modes. *Acta Mater.* **2018**, *152*, 16–33. [[CrossRef](#)]
7. Kofstad, P. *High Temperature Corrosion*; Elsevier Applied Science: London, UK, 1988; ISBN 1-85166-154-9.
8. Rajabinezhad, M.; Bahrami, A.; Mousavinia, M.; Seyedi, S.J.; Taheri, P. Corrosion-Fatigue Failure of Gas-Turbine Blades in an Oil and Gas Production Plant. *Materials* **2020**, *13*, 900. [[CrossRef](#)] [[PubMed](#)]
9. Guo, J.; Cao, T.; Cheng, C.; Meng, X.; Zhao, J. The Relationship Between Magnetism and Microstructure of Ethylene Pyrolysis Furnace Tubes after a Long-term Service. *Microsc. Microanal.* **2018**, *24*, 478–487. [[CrossRef](#)]
10. Takahashi, S.; Sato, Y.; Kamada, Y.; Abe, T. Study of chromium depletion by magnetic method in Ni-based alloys. *J. Magn. Magn. Mater.* **2004**, *269*, 139–149. [[CrossRef](#)]
11. Rahmani, K. Magnetic Property Changes of CoNiCrAlY Coating Under Cyclic Oxidation and Hot Corrosion. *Oxid. Met.* **2020**, *93*, 75–86. [[CrossRef](#)]
12. Mook, G.; Simonin, J.; Feist, W.D.; Hinken, J.H.; Perrin, G. Detection and characterization of magnetic anomalies in gas turbine disks. In Proceedings of the 9th European Conference on NDT, Berlin, Germany, 25–29 September 2006.
13. Aspden, R.G.; Economy, G.; Pement, F.W.; Wilson, I.L. Relationship between magnetic properties, sensitization, and corrosion of incoloy alloy 800 and inconel alloy 600. *Metrics* **1972**, *3*, 2691–2697. [[CrossRef](#)]

14. Schnell, A.; Germerdonk, K.; Antonelli, G. A Non-destructive Testing Method of Determining the Depletion of a Coating. U.S. Patent US7175720B2, 13 February 2007.
15. Fricke, L.V.; Thüerer, S.E.; Jahns, M.; Breidenstein, B.; Maier, H.J.; Barton, S. Non-destructive, Contactless and Real-Time Capable Determination of the α' -Martensite Content in Modified Subsurfaces of AISI 304. *J. Nondestruct. Eval.* **2022**, *41*, 72. [[CrossRef](#)]
16. Mercier, D.; Lesage, J.; Decoopman, X.; Chicot, D. Eddy currents and hardness testing for evaluation of steel decarburizing. *Mater. Sci.* **2006**, *39*, 652–660. [[CrossRef](#)]
17. Stegemann, D.; Reimche, W.; Feiste, K.L.; Heutling, B. Determination of Mechanical Properties of Steel Sheet by Electromagnetic Techniques. In *Nondestructive Characterization of Materials VIII*; Green, R.E., Ed.; Springer: Boston, MA, USA, 1998; pp. 269–275, ISBN 978-1-4613-7198-4.
18. Barton, S.; Zaremba, D.; Maier, H.J. Microstructural degradation in the subsurface layer of the nickel base alloy 718 upon high-temperature oxidation. *Mater. High Temp.* **2021**, *38*, 147–157. [[CrossRef](#)]
19. Barton, S. Zerstörungsfreie Bewertung des Randzonenzustands und Schädigungsgrads in Nickelbasislegierungen Infolge von Hochtemperaturkorrosion. Ph.D. Thesis, Gottfried Wilhelm Leibniz Universität Hannover, Hannover, Germany, TEWISS—Technik und Wissen GmbH, Garbsen, Germany, 2022.
20. Burkhardt, G.L.; Kwun, H. Nonlinear harmonics method and system for measuring degradation in protective coatings. U.S. Patent US19980168185 19981007, 7 October 1998.
21. Guth, S. *Schädigung und Lebensdauer von Nickelbasislegierungen unter Thermisch-Mechanischer Ermüdungsbeanspruchung bei Verschiedenen Phasenlagen*; KIT Scientific Publishing: Karlsruhe, Germany, 2016; ISBN 978-3-7315-0445-0.
22. Deng, W.; Xu, J.; Hu, Y.; Huang, Z.; Jiang, L. Isothermal and thermomechanical fatigue behavior of Inconel 718 superalloy. *Mater. Sci. Eng. A* **2019**, *742*, 813–819. [[CrossRef](#)]
23. Fournier, D.; Pineau, A. Low cycle fatigue behavior of inconel 718 at 298 K and 823 K. *Metall. Mater. Trans. A* **1977**, *8*, 1095–1105. [[CrossRef](#)]
24. Fissolo, A.; Gourdin, C.; Ancelet, O.; Amiable, S.; Demassieux, A.; Chapuliot, S.; Haddar, N.; Mermaz, F.; Stelmaszyk, J.M.; Constantinescu, A. Crack initiation under thermal fatigue: An overview of CEA experience Part II (of II): Application of various criteria to biaxial thermal fatigue tests and a first proposal to improve the estimation of the thermal fatigue damage. *Int. J. Fatigue* **2009**, *31*, 1196–1210. [[CrossRef](#)]
25. Sangid, M.D. The physics of fatigue crack initiation. *Int. J. Fatigue* **2013**, *57*, 58–72. [[CrossRef](#)]
26. Kirka, M.M.; Greeley, D.A.; Hawkins, C.; Dehoff, R.R. Effect of anisotropy and texture on the low cycle fatigue behavior of Inconel 718 processed via electron beam melting. *Int. J. Fatigue* **2017**, *105*, 235–243. [[CrossRef](#)]
27. Droste, M.; Henkel, S.; Biermann, H.; Weidner, A. Influence of Plastic Strain Control on Martensite Evolution and Fatigue Life of Metastable Austenitic Stainless Steel. *Metals* **2022**, *12*, 1222. [[CrossRef](#)]
28. Smaga, M.; Boemke, A.; Daniel, T.; Skorupski, R.; Sorich, A.; Beck, T. Fatigue Behavior of Metastable Austenitic Stainless Steels in LCF, HCF and VHCF Regimes at Ambient and Elevated Temperatures. *Metals* **2019**, *9*, 704. [[CrossRef](#)]
29. Wagenhuber, E.-G.; Trindade, V.B.; Krupp, U. The Role of Oxygen-Grain-Boundary Diffusion During Intercrystalline Oxidation and Intergranular Fatigue Crack Propagation in Alloy 718. In Proceedings of the Symposium on Superalloys 718, 625, 706 and Derivatives, Pittsburgh, PA, USA, 2–5 October 2005; pp. 591–600, ISBN 978-0-87339-602-8.
30. Gustafsson, D.; Moverare, J.; Johansson, S.; Hörnqvist, M.; Simonsson, K.; Sjöström, S.; Sharifimajda, B. Fatigue crack growth behaviour of Inconel 718 with high temperature hold times. *Procedia Eng.* **2010**, *2*, 1095–1104. [[CrossRef](#)]
31. Ghonem, H.; Nicholas, T.; Pineau, A. Elevated temperature fatigue crack growth in alloy 718 part II: Effects of environmental and material variables. *Fatigue Fract. Eng. Mater. Struct.* **1993**, *16*, 577–590. [[CrossRef](#)]
32. Viskari, L.; Hörnqvist, M.; Moore, K.L.; Cao, Y.; Stiller, K. Intergranular crack tip oxidation in a Ni-base superalloy. *Acta Mater.* **2013**, *61*, 3630–3639. [[CrossRef](#)]
33. Leo Prakash, D.G.; Walsh, M.J.; Maclachlan, D.; Korsunsky, A.M. Crack growth micro-mechanisms in the IN718 alloy under the combined influence of fatigue, creep and oxidation. *Int. J. Fatigue* **2009**, *31*, 1966–1977. [[CrossRef](#)]
34. Delaunay, F.; Berthier, C.; Lenglet, M.; Lameille, J.-M. SEM-EDS and XPS Studies of the High Temperature Oxidation Behaviour of Inconel 718. *Mikrochim. Acta* **2000**, *132*, 337–343. [[CrossRef](#)]
35. Sanviemvongsak, T.; Monceau, D.; Desgranges, C.; Macquaire, B. Intergranular oxidation of Ni-base alloy 718 with a focus on additive manufacturing. *Corros. Sci.* **2020**, *170*, 108684. [[CrossRef](#)]
36. Garat, V.; Deleume, J.; Cloue, J.-M.; Andrieu, E. High Temperature Intergranular Oxidation of Alloy 718. In Proceedings of the Symposium on Superalloys 718, 625, 706 and Derivatives, Pittsburgh, PA, USA, 2–5 October 2005; pp. 559–569, ISBN 978-0-87339-602-8.
37. Celada-Casero, C.; Kooiker, H.; Groen, M.; Post, J.; San-Martin, D. In-Situ Investigation of Strain-Induced Martensitic Transformation Kinetics in an Austenitic Stainless Steel by Inductive Measurements. *Metals* **2017**, *7*, 271. [[CrossRef](#)]
38. Cao, B.; Iwamoto, T.; Bhattacharjee, P.P. An experimental study on strain-induced martensitic transformation behavior in SUS304 austenitic stainless steel during higher strain rate deformation by continuous evaluation of relative magnetic permeability. *Mater. Sci. Eng. A* **2020**, *774*, 138927. [[CrossRef](#)]
39. Jones, R. Fatigue crack growth and damage tolerance. *Fatigue Fract. Eng. Mater. Struct.* **2014**, *37*, 463–483. [[CrossRef](#)]

40. Yang, Z.; Lu, S.; Tian, Y.; Gu, Z.; Mao, H.; Sun, J.; Vitos, L. Assessing the magnetic order dependent γ -surface of Cr-Co-Ni alloys. *J. Mater. Sci. Technol.* **2021**, *80*, 66–74. [[CrossRef](#)]
41. Bolzoni, F.; Leccabue, F.; Panizzieri, R.; Pareti, L. Magnetic properties and anisotropy of Co-Cr alloy. *J. Magn. Magn. Mater.* **1983**, *31–34*, 845–846. [[CrossRef](#)]